Published in IET Systems Biology
Received on 15th July 2011
Revised on 2nd May 2012
doi: 10.1049/iet-syb.2011.0050

Special Issue: Modelling Noise in Biochemical Reaction Networks

ISSN 1751-8849

Influence of cell-to-cell variability on spatial pattern formation

B. Greese[1,2,3,*] *K. Wester*[4] *R. Bensch*[5,6] *O. Ronneberger*[5,6] *J. Timmer*[1,2,6,7] *M. Hülskamp*[4] *C. Fleck*[1,2,†]

[1]*Center for Biological Systems Analysis (ZBSA), University of Freiburg, Habsburgerstr. 49, 79104 Freiburg, Germany*
[2]*Institute for Physics, University of Freiburg, Hermann-Herder-Str. 3, 79104 Freiburg, Germany*
[3]*Faculty of Biology, University of Freiburg, Schänzlestr. 1, 79104 Freiburg, Germany*
[4]*Botanical Institute, University of Cologne, Zülpicher Str. 47b, 50674 Köln, Germany*
[5]*Department of Computer Science, University of Freiburg, Georges-Köhler-Allee 052, 79110 Freiburg, Germany*
[6]*BIOSS Centre for Biological Signalling Studies, University of Freiburg, Schänzlestr. 18, 79104 Freiburg, Germany*
[7]*Freiburg Institute for Advanced Studies (FRIAS), University of Freiburg, Albertstr. 19, 79104 Freiburg, Germany*
[*]*The current address of Bettina Greese is Department of Astronomy and Theoretical Physics, Lund University, Sölvegatan 14A, 22362 Lund, Sweden*
[†]*The current address of Christian Fleck is Systems and Synthetic Biology, Wageningen University, Dreijenplein 10, 6703 HB Wageningen, The Netherlands*
E-mail: bettina.greese@thep.lu.se

Abstract: Many spatial patterns in biology arise through differentiation of selected cells within a tissue, which is regulated by a genetic network. This is specified by its structure, parameterisation and the noise on its components and reactions. The latter, in particular, is not well examined because it is rather difficult to trace. The authors use suitable local mathematical measures based on the Voronoi diagram of experimentally determined positions of epidermal plant hairs (trichomes) to examine the variability or noise in pattern formation. Although trichome initiation is a highly regulated process, the authors show that the experimentally observed trichome pattern is substantially disturbed by cell-to-cell variations. Using computer simulations, they find that the rates concerning the availability of the protein complex that triggers trichome formation plays a significant role in noise-induced variations of the pattern. The focus on the effects of cell noise yields further insights into pattern formation of trichomes. The authors expect that similar strategies can contribute to the understanding of other differentiation processes by elucidating the role of naturally occurring fluctuations in the concentration of cellular components or their properties.

1 Introduction

Many spatial patterns arising in biology show remarkably regular features. However, because of the stochastic nature of biological processes, the resulting patterns deviate from a hypothetical perfect pattern. In general, the concept of pattern formation represents a process by which some cells within a population of initially homogeneous cells acquire a specific fate. The basis for differentiation is the communication between cells via non-cell autonomous molecules or direct cell-to-cell contacts that induce regulation of gene expression [1]. Examples for the study of patterning processes using mathematical models are epidermal patterns such as root hairs [2], cell sizes in sepals [3] and hair follicles [4], as well as other biological systems [5–7]. As it is generally difficult to assess patterns accurately and to discriminate between different patterns by visual inspection the use of mathematical methods is necessary [8]. A useful mathematical framework for many applications is reaction-diffusion equations [9], in which cells communicate via diffusive exchange of molecules.

Recently, the study of variance within a system's behaviour became more popular and led to the question about the consequences of noise [10]. However, only a few studies on pattern formation in biology consider models with a stochastic component, for example, the stochastic Boolean network model for root hairs [2], or examine perturbations on biological networks, for example, underlying flower development [11]. The impact of stochastic noise on patterning is examined in various biological systems, for example, the Bicoid morphogen gradient in *Drosophila* [12], the MinCDE protein system in *Escherichia coli* [13], the delta–notch system [14, 15] and the regulation of patterning by small RNAs [16], as well as in chemical systems, for example, the chlorine dioxide-iodine-malonic acid (CDIMA) reaction [17]. As new quantitative data become available and experimental manipulations to verify theoretical predictions are feasible, the aspect of noise in pattern formation is receiving more attention [1, 10, 18]. These advances require quantitative comparisons of spatial patterns in order to evaluate the effect of perturbations. Classifying patterns as similar or different by visual

inspection is not sufficient, mathematical methods that yield robust, testable statements are needed. The general aim of this new approach to developmental biology is a mechanistic understanding of the processes that lead to the experimental observations [18]. Here, we present an approach to analyse the influence of cell noise on spatial pattern formation.

1.1 Sources and effects of noise

Multiple sources and effects of noise have been explored theoretically and have partly been confirmed experimentally [19–22], but it remains challenging to distinguish noise from different sources because of the complexity of intra- and intercellular processes [10]. Noise can arise from fluctuations in, for example, the number of cell components such as ribosomes and amino acids or the number of nutrients in the extracellular environment [10]. Variations in protein copy number can also originate from stochasticity inherent in genetically identical cells [22]. In the context of pattern formation, additional variability can arise from the potentially inaccurate readout of positional information encoded in morphogen gradients [23]. Noise in biochemical systems can be classified into intrinsic and extrinsic depending on whether the stochasticity is within the process of interest or affects it indirectly [10, 24–27]. We focus on the impact of cell-to-cell variability, that is, stochastic differences between cells of the same tissue, on pattern formation. Without a pre-pattern, cells in one tissue are generally identical, but they will at a given time differ slightly in, for example, protein abundance. The specific cellular composition will influence the patterning mechanism as the rates of the processes involved, for example, protein expression, will vary from cell to cell.

1.2 Trichomes as an example

Trichomes (plant hairs) are specialised cells that protrude from the epidermis and form three branches (Fig. 1). They develop on plant surfaces, that is, two-dimensional (2D) domains, which facilitates their observation and statistical analysis. We examine trichomes that arise in the initiation zone [28] near the base of developing leaves. The underlying molecular processes are regulated by GLABRA1 (GL1), GL2, GL3, TRIPTYCHON (TRY) and several homologues [29]. We have established a mathematical model for the interactions of the core patterning genes/proteins [30], which we briefly describe here (Fig. 1*b*). GL1, GL3 and TRY are basally expressed and can be induced by the active complex (AC) that is formed by GL1 and GL3 in some cells. The AC also induces the downstream gene GL2, which triggers the actual differentiation processes. In other cells, TRY and GL3 form an inactive complex, thereby preventing GL2 induction. The inhibitor TRY is the only non-cell autonomous protein in this system. Its mobility therefore represents the intercellular communication. As GL2 is a direct readout of the AC concentration we model only the latter. Hence, trichomes are formed in cells with high AC concentration in the simulation.

1.3 Quantitative analysis

To quantitatively characterise trichome patterns and detect the influence of cell-to-cell variability, appropriate methods are required to describe planar point patterns and determine their degree of regularity. Detecting a deviation from randomness or a difference in point density is not sufficient, subtle differences between relatively similar patterns must be detectable. In addition, we deal with small domains and rather few repetitions. To overcome these limitations, we use tessellation-based methods, which are more sensitive to structural order than, for example, Fourier-based methods [31].

Our approach uses spatial relationships between individuals and their neighbours, which are defined by a modified Delaunay triangulation derived from the Voronoi diagram [32] of the trichomes. We consider neighbours in an appropriate region, that is, neither all others nor only the nearest neighbour, and calculate distances and angles between them as well as the anisotropy of their distribution. Several other studies also present quantifications of spatial patterns based on Voronoi diagrams [8, 31, 33, 34] or related graphs [35–38]. Some also include the definition of graph neighbours [33, 34, 39, 40], which reflects the presumptive short-ranged communication between cells during development [33]. To obtain neighbourhood relationships that reflect a certain morphology, graph edges are sometimes added or deleted, for example, by parameter-dependent

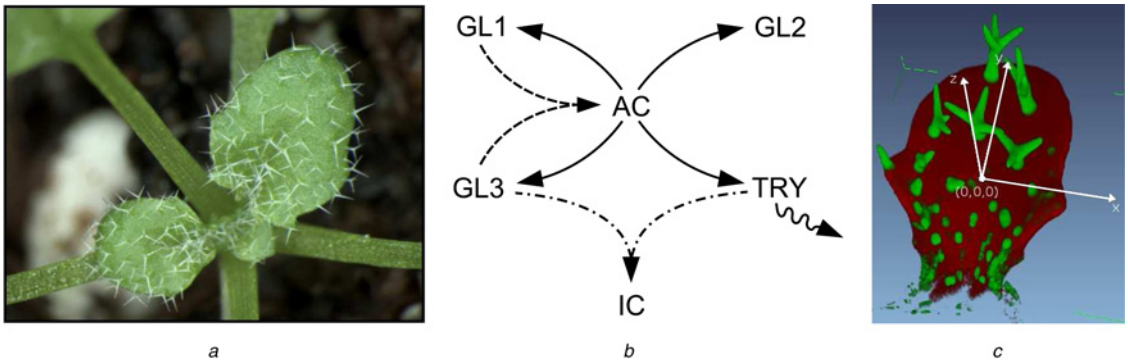

Fig. 1 *Trichomes as an example for pattern formation*

a Trichome distribution over the adaxial (upper) leaf epidermis of *A. thaliana*

b Molecular interactions underlying trichome patterning. GL1 and GL3 bind to form the AC (dashed arrow), which induces GL2 and therefore trichome formation. Alternatively, TRY and GL3 bind to form the inactive complex IC (dash dotted arrow), thereby inhibiting trichome formation. AC regulates the expression of GL1, GL2, GL3, and TRY (solid arrows), and TRY is transported to neighbouring cells (wavy arrow). For clarity, basal expression and degradation are not shown

c Young leaf with mature trichomes and trichome initials. A coordinate system is fitted for labelling. The data volume is obtained from confocal microscopy by stitching together several image stacks

doi: 10.1049/iet-syb.2011.0050

rules [36]. Alternatively, the Gabriel graph [38] is used, which is constructed like the Delaunay triangulation, but with a stricter rule for admissible edges. We use the Gabriel rule to avoid artefacts near the border.

We use these methods to determine the noise level present in our experimental data. This approach is based on the observation that biological patterns often exhibit lattice structures [34]. Similarly to other studies [31, 34], we perform a fit of increasingly irregular hexagon patterns to the trichome data in order to find the best matching pattern and thereby the noise level. Noisy hexagon patterns are well suited for this calibration because they are generic in the sense that they cover the whole range from a regular to a random point pattern [41].

2 Data generation

2.1 Experimental trichome data

We generate two sets of trichome data from rosette leaves of wild-type plants of *Arabidopsis thaliana* (see the Appendix), which differ in their age and shape. One set with 37 flat adult leaves with morphologically visible trichomes is imaged with a light microscope. The base of each trichome is manually labelled in the digital images with ImageJ software (PointPicker plugin), and the labels are saved as 2D coordinates. Another set contains 24 thick and strongly curved young leaves which are rather volumetric than planar objects. In order to visualise those trichomes that only exist as initials within the epidermis, we use a marker line with cell autonomous green fluorescent protein (GFP) expressed in trichomes. The GFP fluorescence and the autofluorescence of the chlorophyll are recorded by confocal laser scanning microscopy. Each young leaf is imaged in several stacks, which are later stitched together to yield a complete data volume [42]. The volumetric leaf surface is extracted and represented as a 2D height field with respect to the leaf's coordinate system (Fig. 1*c*) [43]. As the epidermis lacks chlorophyll, it is not visible in the confocal images. We use the subepidermis to guide the manual labelling of trichome bases in three dimension (3D) using VGStudioMAX (Volume Graphics) and software developed in one of our groups. Notably, the trichome pattern, effectively, is a spatial point pattern on a non-planar surface in space. Hence, we can treat it analogously to all other patterns, with the difference that the neighbourhood relationships and the corresponding measures are calculated in 3D taking the leaf surface into account (see the Appendix). All computations are done with MATLAB (Math Works Inc.). As the data from adult and young leaves do not show any significant difference in the distribution of our measures (not shown), we combine them into one data set with 61 leaves.

2.2 Simulated trichome data

We model the trichome pattern in the initiation zone by four coupled ordinary differential equations, which describe the time evolution of GL1, GL3, TRY and the AC [30]. We consider only those terms that have been found to be relevant and add a transport term for AC to test the influence of its mobility on the pattern. The non-dimensionalised model is given by (1), where [GL1], [GL3], [TRY] and [AC] are the non-dimensional concentrations. Neighbouring cells are coupled by passive transport of TRY and AC, which is defined as

$$\langle [c]_{xy} \rangle = [c]_{x,y-1} + [c]_{x,y+1} + [c]_{x-1,y} + [c]_{x+1,y} + [c]_{x-1,y+1} + [c]_{x+1,y-1} - 6[c]_{xy} \tag{2}$$

where $[c]$ stands for [TRY] or [AC]. We use a discrete hexagonal grid with coordinates $1 \le x \le x_{\max}$ and $1 \le y \le y_{\max}$, a domain of size $D^2 = 50 \times 50$ and zero-flux boundary conditions. The parameters are effective rates that represent basal expression (k_1, k_4), regulated expression (k_2, k_5 and k_{10}), degradation (k_{16}, k_6, k_{11} and k_{14}), complex formation (k_{17} and k_7) and transport (k_{11} k_{13} and k_{14} k_{15}) of the corresponding species. We use the values from our previous parameter scan [30]: $k_1 = 8.2707$, $k_2 = 3.4869$, $k_4 = 15.0952$, $k_5 = 1.3488$, $k_6 = 0.4503$, $k_7 = 7.9509$, $k_{10} = 0.4117$, $k_{11} = 0.9565$, $k_{13} = 10$, $k_{14} = 0.2703$, $k_{16} = 1$ and $k_{17} = 1$. The rate for the activator mobility k_{15} will be varied in order to study the influence of the AC mobility. The initial concentrations are drawn from a normal distribution with mean $[c]_0$ and standard deviation (SD) $0.005[c]_0$, denoted by $\mathcal{N}([c]_0; 0.005[c]_0)$. The concentrations $[c]_0$ represent the stable homogeneous steady state for the different variables. In order to identify [AC] peaks, that is, trichomes, we normalise the final concentrations $[\mathrm{AC}]_{xy}$ by their maximum $[\mathrm{AC}]_{\max}$ and find grid cells with relative concentrations above a threshold of 50%. For each set of conditions, we generate 500 realisations.

2.3 Hexagon and random point patterns

As the generic planar point pattern, we examine hexagon patterns, that is, patterns in which each point is surrounded by six others, including perturbed versions with varying degrees of regularity. We denote the irregular hexagon patterns by $H(\varepsilon)$ where ε denotes the noise level (see the Appendix for details). Fig. 2 shows three examples of $H(\varepsilon)$. The regular arrangement $H(0)$, that is, the deterministic case, represents uniformly packed cells. Strongly disturbed arrangements $H(\varepsilon)$, that is, cases with large stochastic influence, approach a uniformly random pattern and reach it for an SD that is on the order of original inter-point distance [35]. The memory (or recognition) of the initial unperturbed state $H(0)$ is lost well before the patterns $H(\varepsilon)$ and random points get indistinguishable [41]. The coordinates of the random pattern are drawn separately from a random uniform distribution with boundaries 0 and D. We use 110 points, which is the same as in the hexagon patterns.

$$\begin{aligned}
\partial_t[\mathrm{GL1}]_{xy} &= k_1 + k_2[\mathrm{AC}]_{xy} - [\mathrm{GL1}]_{xy}(k_{16} + k_{17}[\mathrm{GL3}]_{xy}) \\
\partial_t[\mathrm{GL3}]_{xy} &= k_4 + k_5[\mathrm{AC}]_{xy} - [\mathrm{GL3}]_{xy}(k_6 + k_{17}[\mathrm{GL1}]_{xy} + k_7[\mathrm{TRY}]_{xy}) \\
\partial_t[\mathrm{TRY}]_{xy} &= k_{10}[\mathrm{AC}]^2_{xy} - [\mathrm{TRY}]_{xy}(k_{11} + k_7[\mathrm{GL3}]_{xy}) + k_{11}k_{13}\langle[\mathrm{TRY}]_{xy}\rangle \\
\partial_t[\mathrm{AC}]_{xy} &= k_{17}[\mathrm{GL1}]_{xy}[\mathrm{GL3}]_{xy} - k_{14}[\mathrm{AC}]_{xy} + k_{14}k_{15}\langle[\mathrm{AC}]_{xy}\rangle
\end{aligned} \tag{1}$$

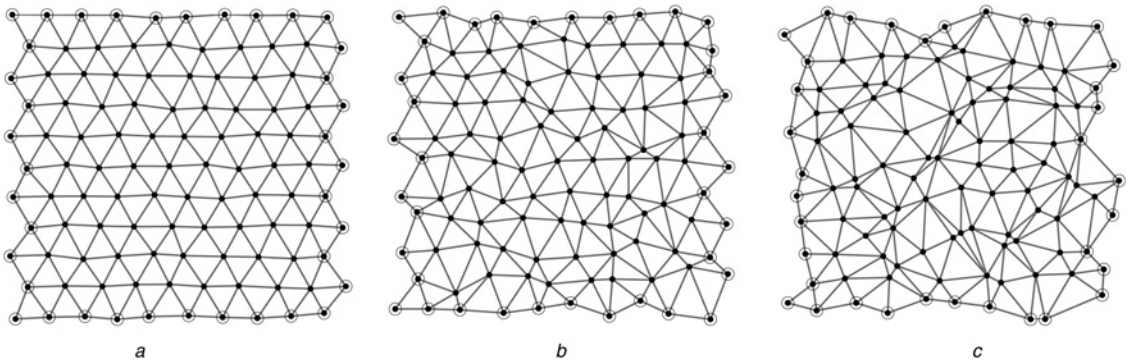

Fig. 2 *Effect of noise ε on hexagon patterns H(ε)*

a $\varepsilon = 0.1$
b $\varepsilon = 0.3$
c $\varepsilon = 0.5$
Edges of the Delaunay triangulation (lines) determine the neighbours of each point. While non-border points (simple dots) have mostly six neighbours around them, the neighbourhood of border points (circled dots) is cut off

3 Method of analysis

3.1 Neighbourhood definition

The local environment around each trichome t_n is determined by the set of its neighbours, which we define by a modified Delaunay triangulation derived from the Voronoi diagram. In a Voronoi diagram $\mathcal{U} = \{V_n\}$, one polygon V_n is constructed around each trichome, which can be interpreted as its influence zone that is determined by the range of the inhibition. By joining all pairs of trichomes whose Voronoi polygons share a edge, we construct the Delaunay triangulation $\mathcal{D}$. The modified triangulation $\mathcal{T}$ is obtained from $\mathcal{D}$ by deleting narrow triangles near the border that are actually artefacts (see Fig. 3*a* and the Appendix). Two trichomes t_{n_1} and t_{n_2} are defined as neighbours if $\mathcal{T}$ contains the edge $\overline{t_{n_1} t_{n_2}}$. The set of neighbours of t_n is denoted by $\mathcal{N}_n$ and the number of neighbours of t_n is denoted by I_n. Owing to the triangulation, the most common case is $I_n = 6$ in general [39], which also holds for noisy hexagon patterns (see the Appendix).

3.2 Neighbourhood measures

While the neighbours have to be determined separately for each realisation k, the neighbourhood measures can be calculated for all trichomes $\{t_n\}_k$ and their respective neighbours together. Hence, we introduce the index m replacing n and k, so that m uniquely labels all trichomes on all leaves of one data set. For each trichome t_m, we calculate the neighbour distances v_i and neighbour angles δ_i by

$$\{v_i\}_m = \{|\overline{t_m t_i}|\}_m \quad \text{and} \quad \{\delta_i\}_m = \{\sphericalangle(t_i, t_m, t_{i+1})\} \tag{3}$$

which equal the edge lengths and interior angles of all triangles involving t_m. For a compact representation, summary statistics can be used (compare [44] for various tessellation-based statistics). Here, we prefer the variation coefficient (VC), that is, the ratio of the SD to the mean, over other summary statistics (see the Appendix). By definition, the VC is normalised and therefore independent of scale or density. The VC is commonly used to measure variability [10] and sometimes even equated with noise [24, 27]. We define the VC for the neighbour angles δ_i by

$$\delta_m^* = \frac{\delta_m^\sigma}{\bar{\delta}_m} \quad \text{with} \quad \bar{\delta}_m = \frac{1}{I_m}\sum_{i=1}^{I_m} \delta_i \quad \text{and}$$
$$\delta_m^\sigma = \sqrt{\frac{1}{I_m - 1}\sum_{i=1}^{I_m} (\delta_i - \bar{\delta}_m)^2} \tag{4}$$

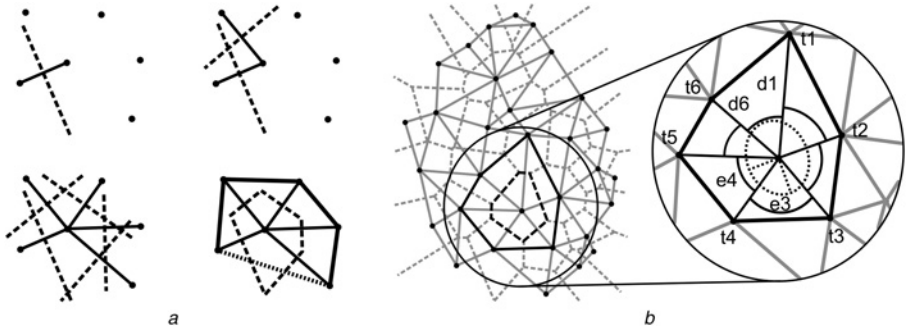

Fig. 3 *Tessellations and neighbour measures*

a Construction of the Voronoi diagram. One line (solid) is drawn between two trichomes and another (dashed) perpendicular to the first at its midpoint. In this manner, the Voronoi polygon (dashed) is constructed around a point. The intersecting lines (solid) are part of the Delaunay triangulation. If the Voronoi polygon (dashed) intersects a line segment (dotted) between adjacent neighbours at the border, the edge is removed in the modified triangulation $\mathcal{T}$
b Voronoi diagram $\mathcal{U}$ (dashed grey lines) and modified triangulation $\mathcal{T}$ (solid grey lines). The neighbourhood relationships are equivalently defined by the Voronoi polygon (dashed black lines) or the intersecting lines of the triangulation (thin black lines). The contiguous Voronoi polygon (thick black lines) is the basis for the calculation of the anisotropy. The ellipse (dotted black) represents the anisotropy, where the principal axes (dotted black lines) correspond to the inverse values of the square root of the eigenvalues (drawn 100-fold longer here for clarity). The trichome in the centre (magnification) has six neighbours t_i. The neighbour distances, for example, v_1 and v_6, and angles, for example, δ_3 and δ_4, (thin black lines and arcs) are the basis for the measures

doi: 10.1049/iet-syb.2011.0050

where $\bar{\delta}_m$ and δ_m^σ are the mean and SD of the neighbour angles at t_m, respectively. We exclude the angle between two border trichomes from our calculations to avoid a bias. The VC for the neighbour distances v_i at t_m, denoted by v_m^*, is defined analogously to (4).

We also characterise the shape of the neighbour distribution $\mathcal{N}_m$ around the corresponding trichome t_m using the polygon with vertices $t_i = (X_i, Y_i) \in \mathcal{N}_m$ (relative to t_m). This contiguous Voronoi polygon [45] is the agglomerate of all Delaunay triangles D_l involving t_m (Fig. 3*b*). Here, we calculate its anisotropy, that is, the dependence of its properties on direction. A well-known measure to detect anisotropy is the moment of inertia tensor [46], which is in 2D defined as

$$A_m = \begin{pmatrix} A_{xx} & A_{xy} \\ A_{xy} & A_{yy} \end{pmatrix} \quad \text{with} \quad A_{xx} = \sum_{i=1}^{I_m} Y_i^2,$$

$$A_{xy} = -\sum_{i=1}^{I_m} X_i Y_i, \quad A_{yy} = \sum_{i=1}^{I_m} X_i^2 \tag{5}$$

Its eigenvalues $\lambda_m^1 \leq \lambda_m^2$ are inversely related to the lengths of the principal axes of an ellipse (Fig. 3*b*). For the special case of an isotropic mass distribution, the principal axes are of equal length so that the ellipse becomes a circle. The ratio of the eigenvalues is a measure for the deviation of the mass distribution from isotropy. Hence, we define the anisotropy of the neighbourhood by

$$a_m = 1 - \frac{\lambda_m^1}{\lambda_m^2} \tag{6}$$

which is bounded by $0 \leq a_m \leq 1$. Applying this concept to contiguous Voronoi polygons means that a_m increases with the noise level ε and effectively measures the deviation from a regular hexagon. We exclude border trichomes from the calculation of a_m to avoid a cut-off effect at the border.

3.3 Noise-induced changes in hexagon patterns

We illustrate the effect of noise on generic planar point patterns by applying our measures to a series of noisy hexagon patterns $H(\varepsilon)$ with $0 \leq \varepsilon \leq 2$ (Fig. 2). We obtain the probability density functions for v_m^*, δ_m^* and a_m by kernel density estimation using a Gaussian kernel function and a bandwidth that is fixed for each statistic. The estimated density curves, denoted by $\hat{f}^{H(\varepsilon)}(\delta^*)$, $\hat{f}^{H(\varepsilon)}(v^*)$ and $\hat{f}^{H(\varepsilon)}(a)$, are shown in the insets in Fig. 4. For increasing ε,

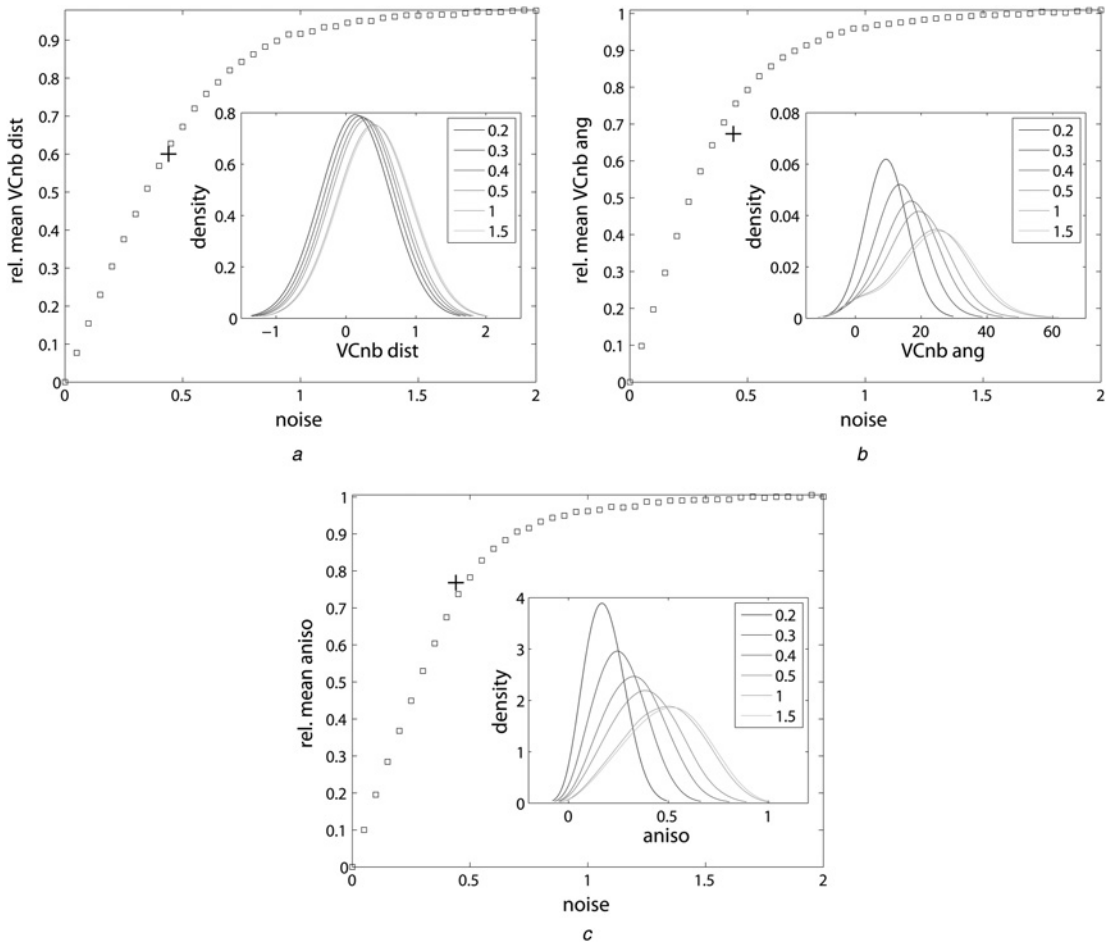

Fig. 4 *Effect of noise ε on hexagon patterns H(ε)*

a VC of the neighbour distances, v_m^*
b VC of the neighbour angles, δ_m^*
c Anisotropy of the neighbourhood, a_m
Main plots show means Φ, Θ and Λ of the measures v_m^*, δ_m^* and a_m, respectively, as functions of ε and relative to $\Phi_R = 0.436$, $\Theta_R = 23.8$ and $\Lambda_R = 0.493$ for the random pattern. The cross corresponds to the value for the experimental pattern, which has the noise level $\varepsilon^* = 0.44$ as determined in Section 4.2. Insets show estimated densities $\hat{f}^{H(\varepsilon)}(v^*)$, $\hat{f}^{H(\varepsilon)}(\delta^*)$ and $\hat{f}^{H(\varepsilon)}(a)$ for selected ε. The errors on the means as determined by a bootstrap with 100 samples are smaller than the symbol height

all $\hat{f}^{H(\varepsilon)}(\cdot)$ become wider and shift towards larger values. In case of v_m^*, this effect is much weaker than for δ_m^* and a_m. For rather large ε, the relevant $\hat{f}^{H(\varepsilon)}(\cdot)$ lie close together and approach $\hat{f}^{R}(\cdot)$ for a uniform random point pattern.

To summarise the density curves and enable easy comparisons, we use the arithmetic means of the three neighbourhood measures defined in (4) and (6). The mean VC of the neighbour angles is given by $\Theta = (1/M)\sum_{m=1}^{M}\delta_m^*$, where M is the total number of trichomes. Analogously, Φ denotes the mean VC of the neighbour distances, v_m^*, and Λ denotes the mean of the anisotropies, a_m. We normalise the measures by Φ_R, Θ_R and Λ_R of the random point pattern. It follows that Φ/Φ_R etc. are zero for perfectly regular and one for random point patterns. In case of $H(\varepsilon)$, the relative quantities Φ/Φ_R, Θ/Θ_R and Λ/Λ_R increase with increasing noise level ε, first roughly linearly and then reaching a saturation level for $\varepsilon > 1$ (main plots in Fig. 4). The behaviour of our chosen measures illustrates that they suit our purpose and quantify the degree of regularity in spatial point patterns.

We now estimate which sample size K is sufficient by comparing $\hat{f}^{H(\varepsilon)}(\delta^*)$, $\hat{f}^{H(\varepsilon)}(v^*)$ and $\hat{f}^{H(\varepsilon)}(a)$ for $\varepsilon = 0.5$ and K varied from 5 to 2000. All curves are very smooth, but those for very small K deviate slightly (not shown). For $K \geq 20$, we find no significant differences in all three $\hat{f}^{H(\varepsilon)}(\cdot)$, so that our chosen standard $K = 500$ for simulations should yield very accurate results. We have $K = 61$ for the experiments, which is well above the threshold.

4 Characterisation of trichome patterning

4.1 Neighbourhood measures

We now calculate the previously discussed measures for our experimental data. The mean number of neighbours is 6.02 ($\pm$0.96) over all trichomes. The distribution of the neighbour counts per leaf shows a dominance of trichomes with six, five and seven neighbours (Fig. 5*a*) with the average of the mean number per leaf being 6.03 ($\pm$0.23). The means of the three neighbourhood measures relative to those for a random pattern are $\Phi/\Phi_R = 0.60$ ($\pm$0.27), $\Theta/\Theta_R = 0.67$ ($\pm$0.41) and $\Lambda/\Lambda_R = 0.77$ ($\pm$0.32) (Fig. 4). Although the trichome differentiation process is governed by a regulatory network, it exhibits significant influence of noise and actually shows a medium degree of regularity that is between a perfectly regular and a random pattern. Hence, we aim to quantify and try to explain this noise by several strategies.

4.2 Noise level

The amount of noise from the various possible contributions is difficult to estimate from experimental data. Instead, we use the noisy hexagon patterns to assess the overall amount of noise present in the observed trichome pattern. For a particular noise level ε, we measure the differences in the distributions of the neighbourhood measures v^*, δ^* and a for the hexagon pattern $H(\varepsilon)$ and the observed trichome patterns. For example, the probability that v^* of $H(\varepsilon)$ lies in a specific interval of size Δv_p^* is given by $\hat{f}_p^{H(\varepsilon)}(v^*)\,\Delta v_p^*$, where $\hat{f}_p^{H(\varepsilon)}(v^*)$ is the estimated probability density function (see Section 3.3) for the step size Δv_p^* at the point p. For the observed trichome patterns, the probability is denoted by $\hat{f}_p(v^*)\,\Delta v_p^*$. We calculate their difference for v^* and analogously for δ^* and a. The sum over the squared differences is taken as the measure for the similarity of $H(\varepsilon)$ and the experimental trichome pattern. Calculating this sum for each ε allows us to find the particular ε^*, for which the patterns are most similar. In effect, we minimise the objective function

$$\begin{aligned}\Delta(\varepsilon) = \sum_{p=1}^{P} [([\hat{f}_p(v^*) - \hat{f}_p^{H(\varepsilon)}(v^*)]\Delta v_p^*)^2 \\ + ([\hat{f}_p(\delta^*) - \hat{f}_p^{H(\varepsilon)}(\delta^*)]\Delta\delta_p^*)^2 \\ + ([\hat{f}_p(a) - \hat{f}_p^{H(\varepsilon)}(a)]\Delta a_p)^2] \end{aligned} \quad (7)$$

The minimum of $\Delta(\varepsilon)$ defines the optimal noise value $\varepsilon^* = \arg\min_\varepsilon \Delta(\varepsilon)$, which reads $\varepsilon^* = 0.44$ in our case (Fig. 5*b*). This means that the generic pattern H (0.44) resembles the observed trichome pattern best.

While this comparison quantifies the noise level in the trichome patterns relative to generic patterns, it remains to be examined what causes this deviation from a regular pattern. Hence, we set out to analyse the source(s) of noise that play a role for the trichome pattern by studying variations of our mathematical model. Our strategy focuses on the effects of spatially different conditions within the simulation domain, which we encode either in the initial states of the cells or the individual reaction rates.

5 Effects of cell noise on trichome patterning

At the onset of trichome initiation, the epidermal tissue consists of identical cells. However, because of the noise

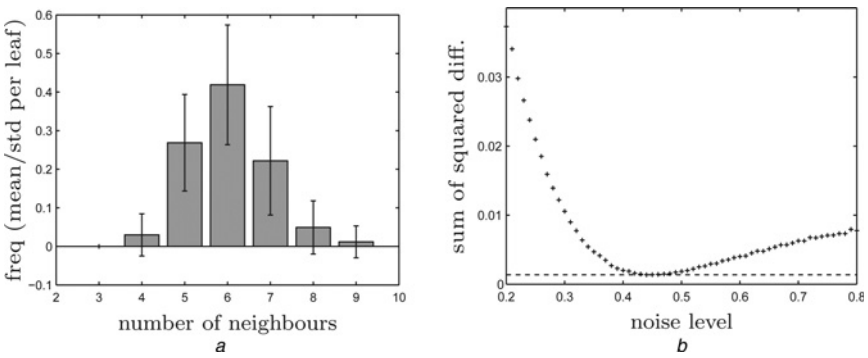

Fig. 5 *Qualitative characterisation of experimental trichome patterns*

a Relative frequency of non-border trichomes with I_m neighbours per leaf. Bar heights represent means and errorbars show SDs

b Objective function $\Delta(\varepsilon)$ for the noise level in the trichome pattern. The minimum at $\varepsilon^* = 0.44$ shows that there is a significant amount of noise present in the experimental pattern

doi: 10.1049/iet-syb.2011.0050

inherent in all biochemical reactions, the actual cell composition will differ slightly from cell to cell. This affects the initial conditions of the patterning system as well as the rates involved in the patterning process. In the following, we separately discuss these two specific sources of spatial variability.

5.1 Random spatially inhomogeneous initial conditions

The trichome initiation process as described by (1) resembles an activator–inhibitor system [47] with an immobile activator. When the simulation of this patterning mechanism starts at time zero, the states of the individual cells differ slightly, which is implemented as random spatially inhomogeneous initial conditions of the differential equations. The development of the pattern, however, is considered to be completely deterministic. The resulting pattern depends only weakly on the initial conditions in case of typical activator–inhibitor systems where both substances are mobile, whereas the dependence becomes strong in case of low activator mobility. In the singular limit of vanishing activator mobility the optimal alignment of the activator peaks is impaired, and noise from the initial conditions remains in the final pattern. A similar effect of very low activator mobility is the formation of asymmetric patterns [48].

We simulate our model first with an immobile AC, that is, $k_{15} = 0$, and then increase k_{15} in steps of 0.005 (Figs. 6*a*–*c*). For small k_{15}, the system exhibits clear AC peaks, representing the trichomes, which get blurred above $k_{15} = 0.075$, when neigbouring cells of a trichome show slightly elevated AC levels. These regions widen until all cells have very similar AC concentrations, that is, the pattern is lost, near $k_{15} = 0.095$. Shortly before, at about $k_{15} = 0.090$, the pattern reaches almost perfect regularity. The transition from very ordered to no pattern happens in a very small range of the parameter k_{15}, where the exact magnitude depends on the chosen discretisation of the mathematical model.

We find by visual inspection that the trichomes are arranged in a more regular fashion when the AC is mobile. The relative mean neighbour measures Φ/Φ_R, Θ/Θ_R and Λ/Λ_R decrease for increasing k_{15} in a slightly sigmoidal fashion (Fig. 6*d*). For a weak AC mobility $k_{15} \leq 0.02$, the pattern is hardly affected, whereas for an intermediate mobility, the regularity increases significantly. This result shows that there is a threshold below which the system behaves the same as for an immobile activator (similar to [48]). Notably, experiments on the trichome patterning system point towards a cell-autonomous AC, that is,

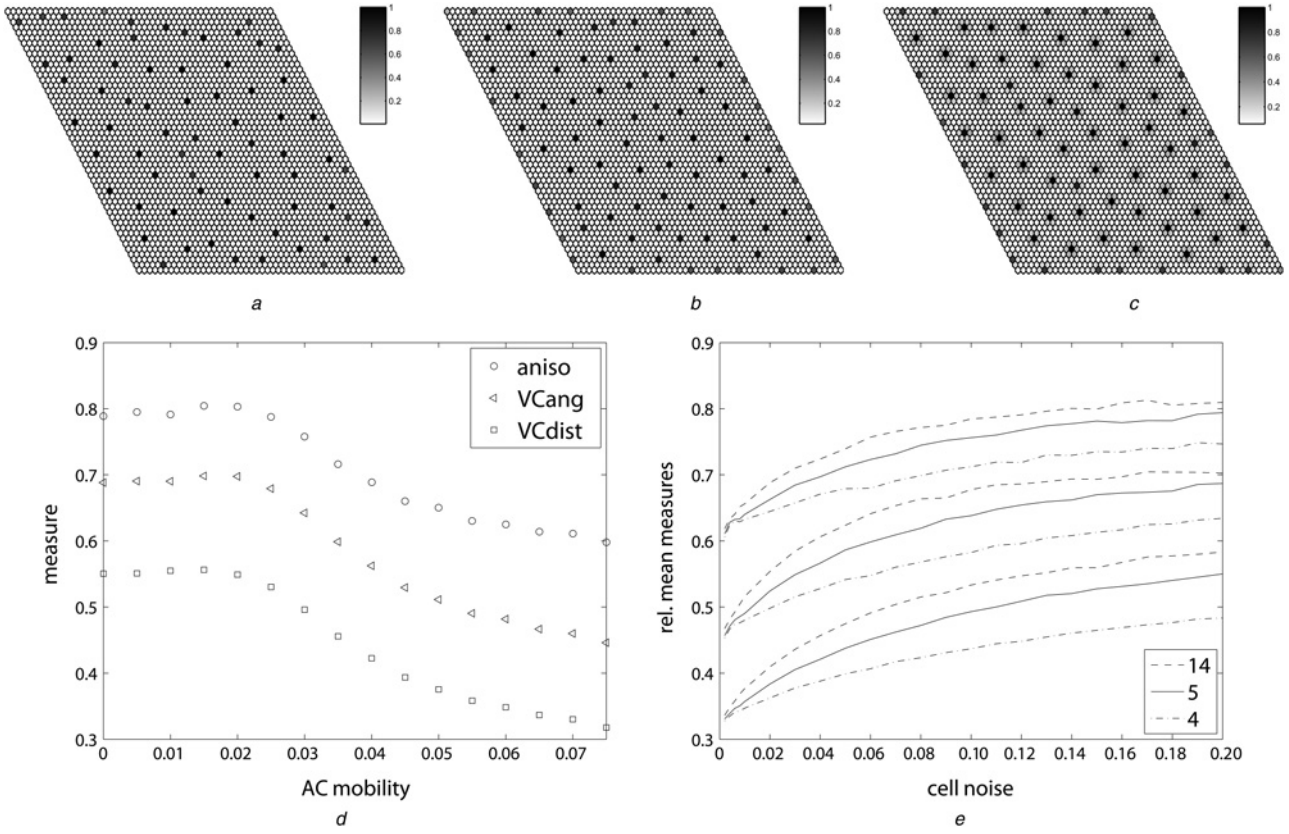

Fig. 6 *Influence of cell noise on the simulated trichome pattern*

a–*c* Simulations with variable mobility of the AC, k_{15} and constant homogeneous parameters
a Immobile AC, that is, $k_{15} = 0$
b Mobile AC with $k_{15} = 0.055$
c Mobile AC with $k_{15} = 0.075$
d Effect of random spatially inhomogeneous initial conditions on the simulated trichome pattern over a range of k_{15}. Plot shows mean values of neighbour measures (relative to a random pattern) against mobility of the AC, k_{15}, which are the relative mean VC of the neighbour distances, Φ/Φ_R (squares), relative mean VC of the neighbour angles, Θ/Θ_R (triangles), and relative mean anisotropy of the neighbourhood, Λ/Λ_R (circles). The errors on the means as determined by a bootstrap with 100 samples are smaller than the symbol height
e Effect of random spatially inhomogeneous parameters on the simulated trichome pattern with mobile AC ($k_{15} = 0.075$). Plot shows mean values of relative neighbour measures against cell noise ε_k: Φ/Φ_R (lower group), Θ/Θ_R (middle group) and Λ/Λ_R (upper group). The line styles correspond to the parameters k_4 (upper group), k_5 (middle group) and k_{14} (lower group). For clarity, the results for k_2, k_7, k_{16} and k_{17} are not shown, these lie between k_5 and k_{14}

$k_{15} = 0$. It follows that the random spatially inhomogeneous initial conditions restrict the regularity of the trichome pattern.

5.2 Random spatially inhomogeneous parameters

Another method to incorporate spatial variability into the simulations is to replace the deterministically fixed rates of the different processes by spatial stochastic fields that represent varying cell compositions. For simplicity, we assume that the correlation time [49] of the cell noise is much larger than the duration of the trichome initiation process, which allows to treat the stochastic rates as time independent.

We perform a systematic analysis of the influence of random parameters on the trichome pattern, in which we simulate the system with only one stochastic parameter at a time to distinguish between the influences of the different processes. All the following simulations are done with zero initial concentrations and mobile AC ($k_{15} = 0.075$) to minimise the dependence on the initial conditions. The stochastic parameter fields $\hat{k}_j^{xy}$ are given by

$$\hat{k}_j^{xy} = k_j + \kappa_{xy} \quad \text{with} \quad \kappa_{xy} \sim \mathcal{N}\left(0; \frac{k_j}{2}\varepsilon_k\right) \tag{8}$$

where k_j is the corresponding deterministic value (given in Section 2.2). This specific choice implies that the cell-individual parameters coincide on average with the constant value used in all other simulations, which reflects our interest in the variability between cells (and not in a shift of the whole process to another parameter value). For each k_j, we generate a series of simulations with $\varepsilon_k = 0.002,\ 0.004,\ \ldots,\ 0.01,\ 0.02,\ \ldots,\ 0.2$, that is, we increase the range of the cell-individual variations. Fig. 6*e* shows the variation of the relative mean neighbour distances Φ/Φ_R and angles Θ/Θ_R as well as the relative mean anisotropy Λ/Λ_R with increasing cell noise ε_k for those parameters that have a significant effect on the regularity of the pattern when they are randomised. For the parameters not shown in the plot, the pattern is rather insensitive to cell noise.

5.2.1 Random expression and degradation rates: Expression and degradation of proteins are both complex sequential biochemical reactions, which are influenced by intrinsic noise. Simulations with cell noise on the corresponding parameters indeed show an influence on the resulting pattern regularity (Fig. 6*e*). In case of k_2 (AC-regulated GL1 expression) and k_5 (AC-regulated GL3 expression), this effect is similar to that of the binding rate for the inactive complex, k_7. The shape of the curves is almost identical. This similarity follows from the fact that these rates influence the abundance of the AC, which determines which cell becomes a trichome and which does not. While the rates k_2 and k_5 are involved in the self-amplification of AC, the rates k_4, k_{14} and k_{16} belong to processes that are independent of the complex formation. The curve corresponding to k_4 (basal GL3 expression) lies well below all others, thereby illustrating a weaker influence of basal expression. The strongest influence is exerted by cell noise on the direct degradation of the activating complex, incorporated by k_{14} (AC degradation). Spatial variation on k_{16} (GL1 degradation) also leads to a rather strong variability, which is identical to that for k_7. The system apparently reacts in the same way to variation in the degradation of one component of the activating complex or the sequestration of the other component by an alternative complex. In both cases, the formation of the activating complex – and hence the pattern – is affected.

5.2.2 Random complex formation rates: It is known that protein-binding rates are strongly influenced by macromolecular crowding [21, 50, 51]. This concept refers to the fact that all cellular components experience non-specific steric repulsion [21, 52]. As the abundance of macromolecules will, in general, slightly differ from cell to cell, the macromolecular crowding will vary and as a consequence also the protein-binding rates. A rough estimate based on Zimmerman and Trach [53] shows that 10% variation in the fraction of the cell occupied by molecules, the volume fraction, can lead to at least 30–40% variation in the protein–protein association rate. A higher density of cell components triggers more binding events, which is due to the fact that the resulting complex is energetically favourable over the single molecules as it occupies a smaller volume in the densely packed cell [21, 50]. In simulations with noisy parameters k_{17} or k_7 (GL1–GL3 or GL3-TRY association, respectively), we see an increase in the relative mean neighbourhood measures Φ/Φ_R, Θ/Θ_R and Λ/Λ_R, that is, pattern variability, for larger cell noise ε_k (Fig. 6*e*). This decrease in the regularity of the pattern illustrates an effect of cell-to-cell variations in the volume fraction.

6 Discussion

6.1 Characteristics of trichome patterns

In previous studies, the trichome pattern on *Arabidopsis* leaves has been analysed by simple approaches that only allow a rough pattern classification. Trichomes were counted along the leaf's proximodistal axis to find that they are spaced regularly at initiation [54]. Non-randomness for trichomes on mature leaves has been detected using the average distance between nearest neighbours, and a minimum distance between trichomes has been found by comparing the numbers of adjacent trichomes that are observed on leaves and expected by chance [55]. The results of our study go beyond these by describing the pattern in a detailed analysis of the spacing of trichomes, their angular structure and the local anisotropy. In particular, we base our measurements on a local environment of each trichome, which represents a suitable adaptation to the biological system.

We find that the trichome pattern is very similar to a hexagon pattern with 44% noise. This medium degree of regularity describes a well-sampled epidermis, which may represent the best compromise for the plant between the regulation effort needed for regular patterning and the potential problems caused by random spacing. Although trichomes can arise closer together or further apart compared to a regular pattern, there is a minimal distance between any two of them. Hence, we hypothesise that the epidermis is divided into quite regular regions of competence, which consist of several cells, and that in each region, one cell differentiates into a trichome. The irregularity in the pattern then represents situations where either the competence region is distorted or where the trichome is not exactly in its centre. Both cases represent a kind of noise that affects the spatial arrangement of trichomes.

doi: 10.1049/iet-syb.2011.0050

6.2 Influence of cell noise on the trichome pattern

In order to shed light on the origin of the observed noise in the trichome pattern, we use simulations to investigate the effect of spatial variability in different molecular interactions, that is, cell noise. In terms of the model, this variability implies random, spatially inhomogeneous initial conditions and renders the reaction rates to be stochastic fields rather then deterministically fixed rates. Notably, the influence of the initial conditions in an activator–inhibitor-related model decreases with an increase in the mobility of the activator. We indeed find that the trichome pattern approaches regularity for increasing AC mobility above a certain threshold, so that additional stochasticity is introduced into the system by the cell autonomy of the AC. Furthermore, the regularity of the trichome pattern decreases with increasing stochasticity of some parameters. This impact is strongest for variations in the rates that affect the formation of the activating complex. Besides other sources of noise, the influence of macromolecular crowding is increasingly studied after being neglected for a long time (compare [52, 56]), but its connection to intracellular reactions is not exactly clear yet. As crowding affects complex formation, the volume fraction, differing slightly from cell to cell, affects the regularity of the resulting pattern. In summary, we point out several potential sources of noise and discuss their influence on the trichome pattern, which may partially explain the observed irregularity.

7 Conclusion

In this study, we present a local analysis of a spatial point pattern and evaluate the influence of cell noise on pattern formation taking the initiation of trichomes as an example. Our mathematical methods are tailored to the requirements of small data sets that result from the observation of developmental processes in plant biology. We take the step from a qualitative to a quantitative description of different planar point patterns, which requires a combination of experimental and theoretical tools. Although we learn from comparing real data to generic patterns how much noise the real system contains, a mathematical model is needed to investigate the contribution from various potentially noisy processes. Comparing simulations that incorporate specific stochastic inputs yields relevant insights concerning the influence of cell noise on trichome patterning. Performance of this kind of joint theoretical–experimental study for other systems will provide further understanding of developing structures in biology.

8 Acknowledgments

The authors thank Alexandra Friede (University of Cologne) for providing several confocal images and Thorsten Schmidt (University of Freiburg) for providing his labelling software. BG and CF were supported by BMBF Freiburg Initiative in Systems Biology 0313921 (FRISYS). BG was supported by the Stiftung der Deutschen Wirtschaft (sdw). MH was supported by the SFB572 DFG Priority Program. This study was supported by the Excellence Initiative of the German Federal and State Governments (EXC 294).

9 References

1 Paldi, A.: 'Stochastic gene expression during cell differentiation: order from disorder?', *Cell Mol. Life Sci.*, 2003, **60**, (9), pp. 1775–1778
2 Savage, N.S., Walker, T., Wieckowski, Y., Schiefelbein, J., Dolan, L., Monk, N.A.M.: 'A mutual support mechanism through intercellular movement of CAPRICE and GLABRA3 can pattern the *Arabidopsis* root epidermis', *PLoS Biol.*, 2008, **6**, (9), p. e235
3 Roeder, A.H.K., Chickarmane, V., Cunha, A., Obara, B., Manjunath, B.S., Meyerowitz, E.M.: 'Variability in the control of cell division underlies sepal epidermal patterning in *Arabidopsis thaliana*', *PLoS Biol.*, 2010, **8**, (5), p. e1000367
4 Sick, S., Reinker, S., Timmer, J., Schlake, T.: 'WNT and DKK determine hair follicle spacing through a reaction-diffusion mechanism', *Science*, 2006, **314**, pp. 1447–1450
5 Othmer, H.G., Painter, K., Umulis, D., Xue, C.: 'The intersection of theory and application in elucidating pattern formation in developmental biology', *Math. Model. Natl. Phenom.*, 2009, **4**, (4), pp. 3–82
6 Reeves, G.T., Muratov, C.B., Schüpbach, T., Shvartsman, S.Y.: 'Quantitative models of developmental pattern formation', *Dev. Cell*, 2006, **11**, (3), pp. 289–300
7 Peltier, J., Schaffer, D.V.: 'Systems biology approaches to understanding stem cell fate choice', *IET Syst. Biol.*, 2010, **4**, (1), pp. 1–11
8 Croxdale, J.L.: 'Stomatal patterning in angiosperms', *Am. J. Bot.*, 2000, **87**, (8), pp. 1069–1080
9 Murray, J.D.: 'Mathematical biology. II: spatial models and biomedical applications. Interdisciplinary applied mathematics' (Springer, New York, 2003, vol. 18, 3rd edn.)
10 Swain, P.S., Longtin, A.: 'Noise in genetic and neural networks', *Chaos*, 2006, **16**, (2), p. 026101
11 Espinosa-Soto, C., Padilla-Longoria, P., Alvarez-Buylla, E.R.: 'A gene regulatory network model for cell-fate determination during *Arabidopsis thaliana* flower development that is robust and recovers experimental gene expression profiles', *Plant Cell*, 2004, **16**, (11), pp. 2923–2939
12 Gregor, T., Wieschaus, E., Mcgregor, A., Bialek, W., Tank, D.: 'Stability and nuclear dynamics of the bicoid morphogen gradient', *Cell*, 2007, **130**, (1), pp. 141–152
13 Howard, M., Rutenberg, A.D.: 'Pattern formation inside bacteria: fluctuations due to the low copy number of proteins', *Phys. Rev. Lett.*, 2003, **90**, (12), p. 128102
14 Ishimatsu, K., Horikawa, K., Takeda, H.: 'Coupling cellular oscillators: a mechanism that maintains synchrony against developmental noise in the segmentation clock', *Dev. Dyn.*, 2007, **236**, (6), pp. 1416–1421
15 Cohen, M., Georgiou, M., Stevenson, N.L., Miodownik, M., Baum, B.: 'Dynamic filopodia transmit intermittent Delta-Notch signaling to drive pattern refinement during lateral inhibition', *Dev. Cell*, 2010, **19**, (1), pp. 78–89
16 Scott, M., Poulin, F.J., Tang, H.: 'Approximating intrinsic noise in continuous multispecies models', *Proc. Royal Soc. A*, 2011, **467**, (2127), pp. 718–737
17 Sanz-Anchelergues, A., Zhabotinsky, A., Epstein, I., Mũnuzuri, A.: 'Turing pattern formation induced by spatially correlated noise', *Phys. Rev. E.*, 2001, **63**, (5), p. 056124
18 Lander, A.D.: 'Pattern, growth, and control', *Cell*, 2011, **144**, (6), pp. 955–969
19 Balázsi, G., van Oudenaarden, A., Collins, J.J.: 'Cellular decision making and biological noise: from microbes to mammals', *Cell*, 2011, **144**, (6), pp. 910–925
20 Eldar, A., Elowitz, M.B.: 'Functional roles for noise in genetic circuits', *Nature*, 2010, **467**, (7312), pp. 167–173
21 Grima, R.: 'Intrinsic biochemical noise in crowded intracellular conditions', *J. Chem. Phys.*, 2010, **132**, (18), p. 185102
22 Kim, P.J., Price, N.D.: 'Macroscopic kinetic effect of cell-to-cell variation in biochemical reactions', *Phys. Rev. Lett.*, 2010, **104**, (14), p. 148103
23 Gregor, T., Tank, D., Wieschaus, E., Bialek, W.: 'Probing the limits to positional information', *Cell*, 2007, **130**, (1), pp. 153–164
24 Elowitz, M.B., Levine, A.J., Siggia, E.D., Swain, P.S.: 'Stochastic gene expression in a single cell', *Science*, 2002, **297**, (5584), pp. 1183–1186
25 Rosenfeld, N., Young, J.W., Alon, U., Swain, P.S., Elowitz, M.B.: 'Gene regulation at the single-cell level', *Science*, 2005, **307**, (5717), pp. 1962–1965
26 Paulsson, J.: 'Summing up the noise in gene networks', *Nature*, 2004, **427**, (6973), pp. 415–418
27 Raser, J.M., O'Shea, E.K.: 'Noise in gene expression: origins, consequences, and control', *Science*, 2005, **309**, (5743), pp. 2010–2013
28 Schnittger, A., Folkers, U., Schwab, B., Jürgens, G., Hülskamp, M.: 'Generation of a spacing pattern: the role of TRIPTYCHON in trichome patterning in *Arabidopsis*', *Plant Cell*, 1999, **11**, (6), pp. 1105–1116

29 Hülskamp, M.: 'Plant trichomes: a model for cell differentiation', *Nat. Rev. Mol. Cell Biol.*, 2004, **5**, (6), pp. 471–480
30 Digiuni, S., Schellmann, S., Geier, F., *et al.*: 'A competitive complex formation mechanism underlies trichome patterning on *Arabidopsis* leaves', *Mol. Syst. Biol.*, 2008, **4**, pp. 217–000
31 Kinney, J.H., Oliveira, J., Haupt, D.L., Marshall, G.W., Marshall, S.J.: 'The spatial arrangement of tubules in human dentin', *J. Mater. Sci. Mater. Med.*, 2001, **12**, (8), pp. 743–751
32 Okabe, A., Boots, B., Sugihara, K., Chiu, S.N.: 'Spatial tessellations: concepts and applications of Voronoi diagrams Wiley series in probability and mathematical statistics' (Wiley, Chichester, 2000, 2nd edn.)
33 Eglen, S.J., Willshaw, D.J.: 'Influence of cell fate mechanisms upon retinal mosaic formation: a modelling study', *Development*, 2002, **129**, pp. 5399–5408
34 Shapiro, M., Schein, S., Monasterio, F.: 'Regularity and structure of the spatial pattern of blue cones of macaque retina', *J. Am. Stat. Assoc.*, 1985, **80**, (392), pp. 803–812
35 Dussert, C., Rasigni, M., Palmari, J., Rasigni, G., Llebaria, A., Marty, F.: 'Minimal spanning tree analysis of biological structures', *J. Theor. Biol.*, 1987, **125**, (3), pp. 317–323
36 Fernandez-Gonzalez, R., Barcellos-Hoff, M.H., de Solórzano, C.O.: 'A tool for the quantitative spatial analysis of complex cellular systems', *IEEE Trans. Image Process.*, 2005, **14**, (9), pp. 1300–1313
37 Jaromczyk, J.W., Toussaint, G.T.: 'Relative neighborhood graphs and their relatives', *Proc. IEEE*, 1992, **80**, (9), pp. 1502–1517
38 Raymond, E., Raphael, M., Grimaud, M., Vincent, L., Binet, J.L., Meyer, F.: 'Germinal center analysis with the tools of mathematical morphology on graphs', *Cytometry*, 1993, **14**, (8), pp. 848–861
39 Duyckaerts, C., Godefroy, G., Hauw, J.J.: 'Evaluation of neuronal numerical density by Dirichlet tessellation', *J. Neurosci. Methods*, 1994, **51**, (1), pp. 47–69
40 Tanemura, M., Honda, H., Yoshida, A.: 'Distribution of differentiated cells in a cell sheet under the lateral inhibition rule of differentiation', *J. Theor. Biol.*, 1991, **153**, pp. 287–300
41 Lucarini, V.: 'From symmetry breaking to Poisson point process in 2D Voronoi tessellations: the generic nature of hexagons', *J. Stat. Phys.*, 2008, **130**, (6), pp. 1047–1062
42 Emmenlauer, M., Ronneberger, O., Ponti, A., *et al.*: 'XuvTools: free, fast and reliable stitching of large 3D datasets', *J. Microsc.*, 2009, **233**, (1), pp. 42–60
43 Bensch, R., Ronneberger, O., Greese, B., *et al.*: 'Image analysis of *Arabidopsis* trichome patterning in 4D confocal datasets', *IEEE Int. Symp. Biomed Imaging*, 2009, pp. 742–745
44 Chiu, S.N.: 'Spatial point pattern analysis by using Voronoi diagrams and Delaunay tessellations – a comparative study', *Biom. J.*, 2003, **45**, (1), pp. 367–376
45 Schaap, W.E., van de Weygaert, R.: 'Continuous fields and discrete samples: reconstruction through Delaunay tessellations', *Astron. Astrophys.*, 2000, **363**, pp. 29–32
46 Goldstein, H., Poole, C., Safko, J.: 'Classical mechanics' (Addison Wesley, San Francisco, 2002, 3rd edn.)
47 Gierer, A., Meinhardt, H.: 'A theory of biological pattern formation', *Kybernetik*, 1972, **12**, pp. 30–39
48 Wei, J., Winter, M.: 'Existence and stability analysis of asymmetric patterns for the Gierer-Meinhardt system', *J. Math Pure Appl. (9)*, 2004, **83**, (4), pp. 433–476
49 Gardiner, C.W.: 'Handbook of stochastic methods of Springer series in synergetics' (Springer, Berlin Heidelberg, 1990, vol. 13, 2nd edn.)
50 Minton, A.P.: 'Influence of macromolecular crowding upon the stability and state of association of proteins: predictions and observations', *J. Pharm. Sci.*, 2005, **94**, (8), pp. 1668–1675
51 Minton, A.P.: 'How can biochemical reactions within cells differ from those in test tubes?', *J. Cell Sci.*, 2006, **119**, (Pt 14), pp. 2863–2869
52 Ellis, R.J.: 'Macromolecular crowding: obvious but underappreciated', *Trends Biochem. Sci.*, 2001, **26**, (10), pp. 597–604
53 Zimmerman, S.B., Trach, S.O.: 'Estimation of macromolecule concentrations and excluded volume effects for the cytoplasm of *Escherichia coli*', *J. Mol. Biol.*, 1991, **222**, (3), pp. 599–620
54 Hülskamp, M., Misera, S., Jürgens, G.: 'Genetic dissection of trichome cell development in *Arabidopsis*', *Cell*, 1994, **76**, (3), pp. 555–566
55 Larkin, J.C., Young, N., Prigge, M., Marks, M.D.: 'The control of trichome spacing and number in *Arabidopsis*', *Development*, 1996, **122**, (3), pp. 997–1005
56 Minton, A.P.: 'The influence of macromolecular crowding and macromolecular confinement on biochemical reactions in physiological media', *J. Biol. Chem.*, 2001, **276**, (14), pp. 10577–10580

10 Appendix

10.1 Details on experimental data

All data are obtained from rosette leaves of wild type *A. thaliana* in the Landsberg erecta ecotype, which contain GFP fused to the endoplasmatic reticulum signal sequence (ER) expressed under the GL2 promotor (pGL2::GFP-ER). This construct marks cells with high GL2 content, that is, trichomes. Plants are grown on soil under long day conditions (16 h light, 8 h dark). We use the third leaf at an age of 8 and 18 days for confocal laser scanning and light microscopy, respectively. The younger leaves are prepared with petioles from seedlings, embedded in 1% MS Agar, and imaged without a cover slip. The older leaves are cut off the plant, incubated in 75% ethanol and 70 °C for 5 min to wash out the chlorophyll, and imaged under a cover slip.

10.2 Calculation of neighbourhood measures from confocal data

A coordinate system is fitted to each leaf such that the origin lies in the centre of mass and the axes are aligned with the natural leaf axes as shown in Fig. 1*c*. If needed, we adjust the 3D labels slightly so that they lie on the leaf surface given by the height field. Then, we obtain the influence zones around each trichome by associating every pixel of the leaf surface with its closest trichome. From this Voronoi-like diagram, we determine the neighbourhood relationships by finding adjacent influence zones. The neighbour distances v_i are calculated by approximating the geodetic distance along the leaf surface using the height field data. We take the angles between the line segments between a trichome and two adjacent neighbours as the neighbour angles δ_i. For the calculation of the anisotropy, we generalise the moment of inertia tensor given in (5) to three dimensions and base the anisotropy on the ratio of the smallest to the medium eigenvalue analogously to (6). Note that the largest eigenvalue is not relevant for our study because its corresponding eigenvector is roughly perpendicular to the leaf surface.

10.3 Construction of hexagon patterns

We use two grid vectors at an angle of 60° to place points in a quadratic domain Ω of size $D^2 = 50 \times 50$ arbitrary units starting from its centre. Adding noise $\eta_n, \xi_n \in \mathbb{R}$ yields

$$(X_n,\ Y_n) = \left(\frac{D}{2} + c_x \boldsymbol{h}_x + \eta_n,\ \frac{D}{2} + c_y \boldsymbol{h}_y + \xi_n\right) \tag{9}$$

with $c_x, c_y \in \mathbb{Z}$. The grid vectors are defined by

$$\boldsymbol{h}_x = (d, 0) \quad \text{and} \quad \boldsymbol{h}_y = \left(\frac{d}{2},\ \frac{\sqrt{3}}{2}\, d\right) \tag{10}$$

where $d = 5$ arbitrary units is the original inter-point distance. We define η_n and ξ_n so that (X_n, Y_n) coincide on average with their original and the perturbations reflect a noise level ε by setting

$$\eta_{\mathrm{n}},\ \xi_{\mathrm{n}} \sim \mathcal{N}\left(0;\ \frac{d}{2}\,\varepsilon\right) \tag{11}$$

This implicit definition of ε uses the fact that 95% of the

doi: 10.1049/iet-syb.2011.0050

values in a normal distribution lie within two SD of its mean. The regular lattice is a special case with $\eta_n = \xi_n = 0$ for all n.

10.4 Construction of the modified triangulation

The Voronoi diagram $\mathcal{U} = \{V_n\}$ and the Delaunay triangulation $\mathcal{D} = \{D_l\}$ are dual tessellations of a domain Ω into non-overlapping and adjacent regions [32]. For $\mathcal{U} = \{V_n\}$, the domain Ω is split into convex polygons V_n by associating all locations $(X,\ Y) \in \Omega$ with their closest trichome(s), that is, one Voronoi polygon V_n is formed around each trichome $t_n = (X_n,\ Y_n)$. For $\mathcal{D} = \{D_l\}$ with $l = 1, \ldots, L_k$, the convex hull of all trichomes is split into L_k triangles D_l by joining all pairs of trichomes whose Voronoi polygons share an edge.

The border B is initially given by the convex hull of the trichomes. We check for each triangle $T_{\mathrm{B}} = \{t_n,\ t_i,\ t_{i'}\}$ that involves at least two border trichomes $t_i,\ t_{i'} \in \mathrm{B}$ whether the line segment $\overline{t_i,\ t_{i'}}$ intersects the Voronoi polygon V_n. If this is true, T_{B} is deleted and B is updated by deleting $\overline{t_i,\ t_{i'}}$ and adding $\overline{t_n,\ t_i}$ and $\overline{t_n,\ t_{i'}}$. This criterion is usually applied to all edges in the Delaunay triangulation $\mathcal{D}$ to obtain the Gabriel graph [38]. We apply our modification step repeatedly until no more unwanted border edges are found, taking care not to completely disconnect any trichome.

10.5 Comparison of different summary statistics for neighbour measures

The mean and median of the neighbour angles δ_i are not appropriate for detecting the noise level because they are interrelated with the number of neighbours per trichome (I_m). This in turn follows a distribution with a peak at $I_m = 6$ for any pattern (shown in Fig. 7 for noisy hexagon patterns $H(\varepsilon)$). Even random point patterns are dominated by points with six neighbours, followed by five and then seven [40]. For each set $\{\delta_i\}_m$ and $\{v_i\}$, we consider the extremes, quartiles, range, and SD, and compare them for a range of noise levels ε (not shown). In both cases, we choose the SD, which is reliable and powerful to distinguish between different ε.

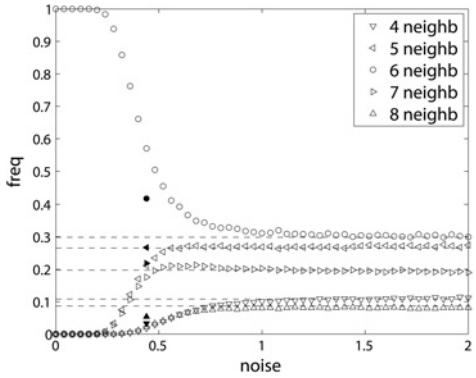

Fig. 7 *Relative frequency of points with I_m neighbours depending on the noise level ε*

Symbols correspond to the number of neighbours I_m
Markers refer to disturbed hexagon patterns $H(\varepsilon)$, the dashed line denotes the level for random point patterns, and filled markers denote the relative frequency for real trichome patterns